Engineering Structures 157 (2018) 235–249

Contents lists available at ScienceDirect

Engineering Structures

journal homepage: www.elsevier.com/locate/engstruct

A new approach to determine strength of Perfobond rib shear connector in steel-concrete composite structures by employing neural network

Hamed Allahyari[a], Iman M. Nikbin[b,*], Saman Rahimi R.[c], Amin Heidarpour[a]

[a] Department of Civil Engineering, Monash University, Melbourne, Australia
[b] Department of Civil Engineering, Rasht Branch, Islamic Azad University, Rasht, Iran
[c] Young Researchers and Elite Club, Rasht Branch, Islamic Azad University, Rasht, Iran

ARTICLE INFO

Keywords:
Shear connector
Sensitivity analysis
ANN
Parametric study
Empirical equation
Composite

ABSTRACT

The main objective of this study is to introduce a novel numerical approach, based on Artificial Neural Network (ANN), to predict the shear strength of Perfobond rib shear connector (PRSC). For this purpose, 90 records were extracted from the literature and were used to develop a number of Bayesian neural network models for predicting the shear strength of PRSC. An accurate ANN model was attained with a high value of correlation coefficient for the train and test subsets. Having a reliable ANN, a parametric study on the shear strength of PRSC was carried out to establish the trend of main contributing factors. The majority of assumptions, considered by empirical equations, were predicted by the developed ANN. Moreover, a sensitivity analysis of input variables was conducted; the outcomes revealed that the area of concrete dowels had the strongest influence on the shear strength of PRSC. Eventually, using the validated ANN, an abundant number of curves (Master Curves) were generated to introduce a user-friendly equation. According to the results, both the ANN model and the proposed equation reflect a higher accuracy than other existing empirical equations.

1. Introduction

In recent decades, steel-concrete composite/hybrid systems have been extensively used in buildings and bridges. The shear connector is an essential element that assures the shear transfer between the steel profile and the concrete slab and also enables the composite action to develop [1–3]. Conventional shear connectors (i.e. Nelson stud) profit from a high degree of automation in workshops or construction sites; nonetheless, such connectors suffer from some limitations in the case of structures subjected to fatigue. [3–5]. Moreover, in comparison to other types of connectors, the resistance of Nelson stud is somewhat limited and leads to girders designed with partial interaction. Given this fact, many researchers have endeavoured to introduce an enhanced shear connector for composite and hybrid systems [6]. The pioneering research is traced back to 1980s. Perfobond, an alternative connector with higher resistance than a stud, was developed in 1987 by the German company Leonhardt, Andra and Partners for the design of the third bridge over the Caroni river, in Venezuela [3,6,7].

From the economic standpoint, Vianna et al. [8] conducted a study comparing the costs of manufacturing steel girders with several types of connectors. The authors reported that using Perfobond connectors in steel-concrete composite systems could result in an economy drive. Vianna et al. [3] also investigated the resistance, ductility and collapse modes of Perfobond and T-Perfobond rib shear connectors. They revealed that PRSC could provide both economical solution and structural efficiency to transfer the shear in composite and hybrid structures.

Oguejiofor & Hosain [2,9] conducted parametric and numerical studies of PRSC on 40 push-out test specimens. The evaluated PRSC was a simple perforated plate incorporating different numbers of holes and transverse rebars, as well as different compressive strength of concrete. The outcome was two expressions, based on regression analysis and finite element method, for predicting the shear capacity of PRSC.

Cândido-Martins et al. [4] experimentally studied the structural response of PRSC. They reported that an increase in the number of holes leads to a higher resistance of PRSC. According to the results, passing the reinforcement bars through the holes led to an increase in both the resistance and ductility of PRSC and a decrease in the uplift displacement. Moreover, Rodrigues and Laím [6] evaluated the effects of the number of holes, the transverse reinforcement bars in rib holes, and the doubled PRSC at the room and elevated temperatures. The results showed the adverse impact of elevated temperature on the load-carrying capacity of PRSC, particularly, on that of doubled PRSC. They

* Corresponding author.
E-mail addresses: hamed.allahyari@monash.edu (H. Allahyari), Nikbin@iaurasht.ac.ir (I. M. Nikbin), saman.r.r.ac@gmail.com (S. Rahimi R.), amin.heidarpour@monash.edu (A. Heidarpour).

https://doi.org/10.1016/j.engstruct.2017.12.007
Received 30 June 2017; Received in revised form 31 October 2017; Accepted 5 December 2017
Available online 22 December 2017

Nomenclature

f_c	concrete cylinders compressive strength (MPa)
A_{tr}	total area of transverse reinforcement bars (mm^2)
$A_{tr,r}$	area of transverse reinforcement bars in rib holes (mm^2)
A_b	cross-section of the connector at the end-bearing zone (mm^2)
A_{cc}	longitudinal concrete shear area per connector (mm^2)
A_D	total area of concrete dowels (mm^2)
n	number of rib holes
A_F	contact area between the concrete and the connector (mm^2)
h_{sc}	connector height (mm)
h	slab length in the front of connector (mm)
b	concrete slab thickness (mm)
b_f	width of the steel section flange (mm)
L_c	contact length between the concrete and the flange of the steel section
D	connector hole diameter (mm)
D_s	the diameter of the transverse rebar (mm)
f_u	the tensile strength of the transverse rebar (MPa)
α	coefficient of end-bearing force ($\alpha = 1$ and $\alpha = 0$ includes and excludes the end-bearing force, respectively)
t_{sc}	connector thickness (mm)
$f_{y,r}$	yield stress of reinforcement bars in rib holes (MPa)
f_y	yield stress of the transverse rebars (MPa)
q_{exp}	Perfobond connector experimental shear strength (kN)
q_u	Perfobond connector nominal shear strength (kN)
ω_j	weights of network
e_i	errors of network
t_i	targets of network
α_i	outputs of network
γ	performance ratio
mse	the mean square error of the network
msw	the sum of squares of the network weights and biases
σ	standard deviation
COV	coefficient of variation
μ	mean value

List of acronyms

PRSC	Perfobond Rib Shear Connector
ANN	Artificial Neural Network
NMSE	Normalised Mean Square Error
BRB	Bayesian Regularisation Backpropagation

revealed that the presence of transverse reinforcement bars in rib holes reduces the load-carrying capacity of PRSC at elevated temperature. Furthermore, Al-Darzi et al. [10] conducted a parametric study on the shear strength of PRSC, using finite element method. The model was verified by experimental push-out test results, and the results of the parametric study were used to introduce a mathematical model to estimate the shear capacity of PRSC.

Ahn et al. [11] evaluated the shear behaviour of PRSC under the static and cyclic loadings. The results of static tests indicated that the shear capacity of specimens with the pure concrete dowels is about 65% of the shear capacity of specimens with both concrete dowels and concrete end-bearing zone. The shear capacity of specimens with transverse rebars in the holes was also about two times of the shear capacity of specimens with transverse rebars. According to cyclic tests, the residual shear capacity of specimens without transverse rebars was significantly lower than that of static shear capacity. Conversely, the residual shear capacity of specimens with transverse rebars was very close to their static shear capacity.

Zheng et al. [12] conducted a parametric study of circular-hole and long-hole PRSC. The results showed that the failure mode of both circular-hole and long-hole PRSC are associated with concrete failure. They also disclosed that the shear stiffness of PRSC increases with hole diameter and height.

Moreover, Allahyari et al. [13] investigated the dynamic characteristics of steel-concrete decks with PRSC, including normal-weight high-strength concrete and lightweight high-strength concrete. Some dynamic properties such as natural frequencies, damping ratio, and frequency response functions were evaluated through a non-destructive technique. They also compared the experimental results of natural frequencies with the finite element model. The results indicated that the most effective mode was the first mode with a damping ratio of almost 0.5% for both types of concrete.

According to the literature, there are many contributing factors in structural behaviour of PRSC, including the concrete compressive strength, the area and the yield strength of transverse rebars, the end-bearing force, rib arrangement, and rib spacing. Having taken different factors into account, some analytical models have been proposed to predict the resistance of PRSC, although the majority of them suffer from a low accuracy. Today, new models that are easier, convenient, and more accurate than the existing models could develop on account of the recent advances in data analysis techniques.

When coming to the data modelling of nonlinear problems, the traditional regression analysis is of hopeless inadequacy. By contrast, ANN is a powerful data modelling tool that is capable of coping with complex input-output problems. In other words, the power of ANNs lies in the capability to detect and learn nonlinear relations from the collected data. Recent studies have proved that ANN-based modelling is an alternative approach to modelling complex nonlinear problems. As a consequence, ANN-based modelling has rapidly developed in a variety of fields encompassing engineering, psychology, business, medicine, science, and many others. Take, as an illustration, in civil engineering, ANNs have been successfully used to model some behaviour of structures or some characteristics of materials [14–16].

From the literature, attempts to reach an accurate prediction for the shear strength of PRSC is an ongoing process. Therefore, the present study aims at (1) a test for feasibility of employing ANNs for modelling the PRSC, (2) a test for accuracy of other existing empirical equations, (3) a test for sensitivity of the designed ANN to input variables, (4) a parametric study of the PRSC and, eventually, (5) the presentation of a user-friendly equation with the assistance of ANNs.

2. Analytical models to predict the shear strength of PRSC

To evaluate the shear strength of a PRSC (Fig. 1), Oguejiofor and

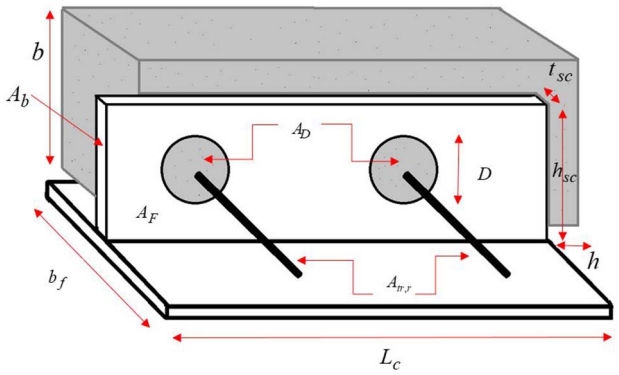

Fig. 1. A schematic of a PRSC.

Hosain [9] proposed a model (Eq. (1)) that takes account of three contributions in the overall shear strength: concrete resistance at the end-bearing zone, the transverse reinforcement bars, and the concrete dowels formed through the holes of the connector:

$$q_u = 0.59A_{cc}\sqrt{f_c} + 1.233A_{tr}f_y + 2.871nD^2\sqrt{f_c} \quad (1)$$

$$q_u = 4.5h_{sc}t_{sc}f_c + 0.91A_{tr}f_y + 3.31nD^2\sqrt{f_c} \quad (2)$$

where q_u is PRSC's nominal shear strength (kN); A_{cc} is the longitudinal shear area of concrete per connector (mm^2); D is the hole diameter (mm); n is the number of holes; h_{sc} is the PRSC's height (mm); t_{sc} is the PRSC's thickness (mm); f_c is the concrete compressive strength (MPa); f_y is the yield stress of the transverse rebars (MPa); A_{tr} is the total area of transverse rebars (mm^2).

Ahn et al. [17] modified Eq. (2) and proposed Eq. (3) to predict the shear strength of Perfobond Connectors.

$$q_u = 3.14h_{sc}t_{sc}f_c + 1.21A_{tr,r}f_{y,r} + 2.98nD^2\sqrt{f_c} \quad (3)$$

where $A_{tr,r}$ is the area of transverse rebars in the rib holes (mm^2).

Medberry and Shahrooz [18] added the chemical bond effects (the second term) to the three parameters of Oguejiofor and Hosain as follows:

$$q_u = 0.747bh\sqrt{f_c} + 0.413b_fL_c + 0.9A_{tr}f_y + 1.66n\pi\left(\frac{D}{2}\right)^2\sqrt{f_c} \quad (4)$$

where h is the slab length in the front of connector (mm); b is the thickness of slab (mm); b_f is the width of the steel section flange (mm); L_c is the contact length between the concrete and the flange of the steel section (mm).

Veríssimo et al. [19] altered the Eq. (2) and proposed Eq. (5) for the estimation of the shear strength of the PRSC:

$$q_u = 4.04\frac{h_{sc}}{b}h_{sc}t_{sc}f_c + 2.37nD^2\sqrt{f_c} + 0.16A_{cc}\sqrt{f_c} + 31.85\times10^6\frac{A_{tr}}{A_{cc}} \quad (5)$$

Al-Darzi et al. [20] presented Eq. (6):

$$q_u = 255.31 + 7.62\times10^{-4}\times h_{sc}t_{sc}f_c - 7.59\times10^{-7}A_{tr}f_y + 3.97\times10^{-3}\times nD^2\sqrt{f_c} \quad (6)$$

Hosaka et al. [21] proposed Eqs. (7) and (8) for PRSC without and with a transverse rebar in the hole, respectively. In these equations ($q_{u,hole}$) takes the contribution of holes into account:

$$q_{u,hole} = 3.38D^2\sqrt{\frac{t_{sc}}{D}}f_c - 39\times10^3 \quad (7)$$

$$q_{u,hole} = 1.45[(D-D_s)f_c + D_s^2f_u] - 26.1\times10^3 \quad (8)$$

where f_u is the tensile strength of the transverse rebar (MPa), and D_s is the diameter of transverse rebars.

According to Cândido-Martins et al. [4], Eq. (2) presented by Oguejiofor and Hosain [9] leads to an unsafe prediction, with an error up to 32%, and overestimates the shear capacity of PRSC. Moreover, Eq. (4) proposed by Medberry and Shahrooz [18] overestimates the resistance of PRSC and provides an unsafe prediction (with an error up to 35%), especially, for those connectors with fewer holes. Eq. (5) is also unsafe; however, it has better accuracy than Eqs. (2) and (5). The model suggested by Hosaka et al. [21] significantly overestimates the proportion of holes in the shear capacity of PRSC. Eventually, the equation presented by Al-Darzi et al. [20] provides a safe estimation and reasonable accuracy for reinforced PRSC; nevertheless, it is unsafe in terms of unreinforced PRSC, with an error about 12%.

As PRSC is a recently developed connector, there is no particular formula in valid standards or guidelines [22]; however, some codes such as Eurocode imposes overall restrictions on the slip of steel-concrete composite structures. Therefore, proposing a more accurate formula for design of PRSC is of particular interest.

3. Artificial neural network

3.1. Background

In recent years, a wave of enthusiasm for human-inspired networks such as social networks, artificial neural networks, and many other networks have been seen. The main feature of these networks is to be capable of classifying data and determining the complex relationships between inputs and outputs. An ANN is a sophisticated mathematical model, inspired by biological neurones and a parallel information processing array to make a decision in a prompt way [23–25].

Biological neurones are in contact with one another via some electrical stimulus called synapse. In other words, communicational signals are constantly generated by a chemical reaction and delivered to other neurones by a synapse. The nerve systems in the human body are made up of an array of layers consisting of such neurones and are able to learn, recall, and generate outputs. Likewise, a synaptic activity is adopted in the process used by ANNs through a matrix containing weights (numerical values); that is, computational neurones are in contact with each other by means of the weight matrix. This matrix is continuously updated and adjusted during the learning process to reach the minimum error of prediction. Therefore, each neurone has a set of weighted inputs, a bias term, and a transfer function describing how the sum of weighted inputs and bias terms is converted to an output [26]. In other words, ANN is inspired by the human brain metaphor, which provides knowledge acquisition through a learning process, and connections between neurones (weight matrix) are used to store the knowledge [27,28]. Fig. 2 illustrates a basic model of a neurone.

Due to the great capability of ANNs in learning complex relationships without prior knowledge of the model, there has been a mounting interest in the employment of these networks in numerical modelling and engineering problem solving [29]. For instance, Hegazy et al. [30] adopted ANNs in predicting the load-deflection behaviour of concrete slabs; Elshafey et al. [31–33] used ANNs for predicting of damage detection in offshore structures, punching-shear of two-way slabs, and crack width in concrete; Cascardi et al. [26] employed ANNs for prediction of compressive strength of FRP-confined concrete circular columns; and Fahmy et al. [34] used ANNs in the design of orthotropic bridge decks.

3.2. Bayesian regularisation framework

Overfitting is a common problem occurring within neural network training. In this case, the network has a negligible error to do with the training subset; however, the error is high when the network encounters new data. In other words, the network has memorised the training examples whereas it has not learned to generalise the principle to new data. Using a large enough network is one of the methods of improving network generalisation; nevertheless, regarding a particular problem, it is hard to know ahead of time how large a network should be [35].

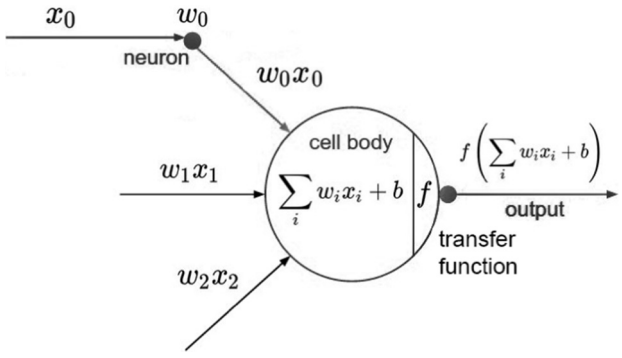

Fig. 2. Basic model of a neuron with three inputs.

Table 1
Data list.

No.	f_c	A_D	n	$A_{tr,r}f_{y,r}$	$A_{tr}f_y$	$A_b = t_{sc}h_{sc}$	b/h_{sc}	h_{sc}	A_F	α	q_{exp}	Ref.
1	28.10	9503.32	4.00	281486.70	351858.38	774.00	1.64	129.00	112993.36	1.00	539.53	[26]
2	32.70	9503.32	4.00	281486.70	351858.38	774.00	1.64	129.00	112993.36	1.00	590.65	
3	41.50	9503.32	4.00	281486.70	351858.38	774.00	1.64	129.00	112993.36	1.00	620.55	
4	52.60	9503.32	4.00	281486.70	351858.38	774.00	1.64	129.00	112993.36	1.00	692.20	
5	26.00	1924.23	2.00	0.00	345575.19	990.60	1.57	76.20	25923.55	1.00	326.83	[3]
6	26.00	1924.23	2.00	0.00	345575.19	1950.00	1.33	150.00	52491.55	1.00	450.20	
7	20.91	0.00	0.00	0.00	0.00	1651.00	1.20	127.00	100125.00	1.00	179.40	[9]
8	20.91	3926.99	2.00	0.00	0.00	1651.00	1.20	127.00	92271.02	1.00	249.10	
9	20.91	5890.49	3.00	0.00	0.00	1651.00	1.20	127.00	88344.03	1.00	274.00	
10	20.91	7853.98	4.00	0.00	0.00	1651.00	1.20	127.00	84417.04	1.00	276.50	
11	20.91	0.00	0.00	0.00	100515.26	1651.00	1.20	127.00	100125.00	1.00	292.00	
12	20.91	3926.99	2.00	0.00	100515.26	1651.00	1.20	127.00	92271.02	1.00	375.20	
13	20.91	5890.49	3.00	0.00	100515.26	1651.00	1.20	127.00	88344.03	1.00	393.60	
14	20.91	7853.98	4.00	0.00	100515.26	1651.00	1.20	127.00	84417.04	1.00	363.70	
15	34.05	0.00	0.00	0.00	100515.26	1651.00	1.20	127.00	100125.00	1.00	396.10	
16	41.43	3926.99	2.00	0.00	100515.26	1651.00	1.20	127.00	92271.02	1.00	563.00	
17	41.43	5890.49	3.00	0.00	100515.26	1651.00	1.20	127.00	88344.03	1.00	597.80	
18	41.43	7853.98	4.00	0.00	100515.26	1651.00	1.20	127.00	84417.04	1.00	595.90	
19	41.43	0.00	0.00	0.00	100515.26	1651.00	1.20	127.00	100125.00	1.00	431.00	
20	41.43	3926.99	2.00	0.00	100515.26	1651.00	1.20	127.00	92271.02	1.00	528.10	
21	41.43	5890.49	3.00	0.00	100515.26	1651.00	1.20	127.00	88344.03	1.00	584.90	
22	41.43	7853.98	4.00	0.00	100515.26	1651.00	1.20	127.00	84417.04	1.00	577.00	
23	24.82	0.00	0.00	0.00	725284.85	1651.00	1.20	127.00	100125.00	1.00	240.70	
24	24.82	3926.99	2.00	0.00	725284.85	1651.00	1.20	127.00	92271.02	1.00	304.90	
25	24.82	5890.49	3.00	0.00	725284.85	1651.00	1.20	127.00	88344.03	1.00	343.80	
26	24.82	7853.98	4.00	0.00	725284.85	1651.00	1.20	127.00	84417.04	1.00	364.70	
27	24.82	0.00	0.00	0.00	821040.59	1651.00	1.20	127.00	100125.00	1.00	413.50	
28	24.82	3926.99	2.00	0.00	821040.59	1651.00	1.20	127.00	92271.02	1.00	533.10	
29	24.82	5890.49	3.00	0.00	821040.59	1651.00	1.20	127.00	88344.03	1.00	580.90	
30	24.82	7853.98	4.00	0.00	821040.59	1651.00	1.20	127.00	84417.04	1.00	577.90	
31	27.49	5890.49	3.00	0.00	803023.82	1651.00	1.20	127.00	88611.03	1.00	543.20	
32	27.49	5890.49	3.00	0.00	803023.82	1651.00	1.20	127.00	88611.03	1.00	554.20	
33	27.49	5890.49	3.00	0.00	707268.08	1651.00	1.20	127.00	88611.03	1.00	349.80	
34	27.49	5890.49	3.00	0.00	707268.08	1651.00	1.20	127.00	88611.03	1.00	345.90	
35	25.97	5890.49	3.00	31918.58	771105.24	1651.00	1.20	127.00	88611.03	1.00	464.40	
36	25.97	5890.49	3.00	31918.58	771105.24	1651.00	1.20	127.00	88611.03	1.00	435.50	
37	26.85	5890.49	3.00	31918.58	771105.24	1651.00	1.20	127.00	88611.03	1.00	544.10	
38	26.85	5890.49	3.00	31918.58	771105.24	1651.00	1.20	127.00	88611.03	1.00	502.20	
39	27.52	3926.99	2.00	0.00	771105.24	1651.00	1.20	127.00	59163.02	1.00	398.60	
40	27.52	3926.99	2.00	0.00	771105.24	1651.00	1.20	127.00	92271.02	1.00	432.50	
41	27.52	3926.99	2.00	0.00	803023.82	1651.00	1.20	127.00	59163.02	1.00	471.80	
42	27.52	3926.99	2.00	0.00	803023.82	1651.00	1.20	127.00	92271.02	1.00	493.20	
43	26.28	3926.99	2.00	0.00	803023.82	1651.00	1.20	127.00	59163.02	1.00	485.80	
44	26.28	3926.99	2.00	31918.58	771105.24	1651.00	1.20	127.00	59163.02	1.00	477.30	
45	26.28	5890.49	3.00	0.00	803023.82	1651.00	1.20	127.00	88611.03	1.00	552.00	
46	26.28	5890.49	3.00	31918.58	771105.24	1651.00	1.20	127.00	88611.03	1.00	533.10	
47	31.00	0.00	0.00	0.00	345575.19	1500.00	1.50	100.00	66650.00	1.00	283.51	[4]
48	31.00	706.86	1.00	0.00	345575.19	1500.00	1.50	100.00	65236.28	1.00	309.44	
49	31.00	1413.72	2.00	0.00	345575.19	1500.00	1.50	100.00	63822.57	1.00	317.52	
50	31.00	2120.58	3.00	0.00	345575.19	1500.00	1.50	100.00	62408.85	1.00	331.35	
51	31.00	2827.43	4.00	0.00	345575.19	1500.00	1.50	100.00	60995.13	1.00	354.03	
52	31.00	706.86	1.00	62203.53	345575.19	1500.00	1.50	100.00	65236.28	1.00	365.93	
53	31.00	706.86	1.00	172787.60	345575.19	1500.00	1.50	100.00	65236.28	1.00	395.68	
54	27.90	0.00	0.00	0.00	0.00	137.50	3.60	25.00	11100.00	0.00	13.14	[1]
55	27.90	283.53	1.00	0.00	0.00	137.50	3.60	25.00	10532.94	0.00	29.48	
56	27.90	567.06	2.00	0.00	0.00	137.50	3.60	25.00	9965.89	0.00	47.38	
57	27.90	850.59	3.00	0.00	0.00	137.50	3.60	25.00	9398.83	0.00	61.20	
58	27.90	1134.11	4.00	0.00	0.00	137.50	3.60	25.00	8831.77	0.00	79.24	
59	27.90	283.53	1.00	35342.92	0.00	137.50	3.60	25.00	10532.94	0.00	49.25	
60	27.90	567.06	2.00	70685.83	0.00	137.50	3.60	25.00	9965.89	0.00	79.39	
61	27.90	850.59	3.00	106028.75	0.00	137.50	3.60	25.00	9398.83	0.00	119.85	
62	27.90	283.53	1.00	35342.92	0.00	137.50	3.60	25.00	10532.94	0.00	39.98	
63	27.90	283.53	1.00	59729.53	0.00	137.50	3.60	25.00	10532.94	0.00	55.29	
64	27.90	283.53	1.00	90477.87	0.00	137.50	3.60	25.00	10532.94	0.00	89.16	
65	26.00	1413.72	2.00	0.00	302378.29	1200.00	1.88	80.00	49672.57	1.00	280.05	[5]
66	26.00	1413.72	2.00	124407.07	302378.29	1200.00	1.88	80.00	49672.57	1.00	398.86	
67	51.90	0.00	0.00	0.00	388772.09	952.50	1.57	76.20	29682.00	1.00	319.28	[18]
68	51.90	1924.23	2.00	0.00	388772.09	952.50	1.57	76.20	25833.55	1.00	344.85	
69	51.90	1924.23	2.00	86393.80	388772.09	952.50	1.57	76.20	25833.55	1.00	443.03	
70	51.90	0.00	0.00	0.00	388772.09	1875.00	1.33	150.00	56250.00	1.00	495.00	
71	51.90	1924.23	2.00	0.00	388772.09	1875.00	1.33	150.00	52401.55	1.00	501.48	
72	51.90	1924.23	2.00	86393.80	388772.09	1875.00	1.33	150.00	52401.55	1.00	549.70	

(continued on next page)

Table 1 (*continued*)

No.	f_c	A_D	n	$A_{tr,r}f_{y,r}$	$A_{tr}f_y$	$A_b = t_{sc}h_{sc}$	b/h_{sc}	h_{sc}	A_F	α	q_{exp}	*Ref.*
73	26.60	0.00	0.00	0.00	876251.51	1651.00	1.20	127.00	100125.00	1.00	384.60	[2]
74	26.60	5890.49	3.00	0.00	876251.51	1651.00	1.20	127.00	88344.03	1.00	568.00	
75	26.60	7853.98	4.00	0.00	876251.51	1651.00	1.20	127.00	84417.04	1.00	585.40	
76	26.60	9817.48	5.00	187710.16	876251.51	1651.00	1.20	127.00	80490.05	1.00	774.20	
77	26.60	0.00	0.00	0.00	876251.51	1651.00	1.20	127.00	46725.00	1.00	373.70	
78	26.60	0.00	0.00	0.00	876251.51	762.00	1.20	127.00	97500.00	1.00	305.90	
79	26.60	5890.49	3.00	0.00	876251.51	762.00	1.20	127.00	85719.03	1.00	448.40	
80	26.60	7853.98	4.00	0.00	876251.51	762.00	1.20	127.00	81792.04	1.00	447.40	
81	26.60	9817.48	5.00	187710.16	876251.51	762.00	1.20	127.00	77865.05	1.00	536.60	
82	26.60	0.00	0.00	0.00	876251.51	762.00	1.20	127.00	45500.00	1.00	282.00	
83	26.60	0.00	0.00	0.00	876251.51	1326.00	1.49	102.00	81375.00	1.00	338.80	
84	26.60	5890.49	3.00	0.00	876251.51	1326.00	1.49	102.00	69594.03	1.00	520.60	
85	26.60	5890.49	3.00	0.00	876251.51	1326.00	1.49	102.00	69594.03	1.00	713.40	
86	26.60	7853.98	4.00	0.00	876251.51	1326.00	1.49	102.00	65667.04	1.00	569.40	
87	26.60	7853.98	4.00	150168.13	876251.51	1326.00	1.49	102.00	65667.04	1.00	764.20	
88	26.60	0.00	0.00	0.00	876251.51	612.00	1.49	102.00	78750.00	1.00	282.50	
89	26.60	5890.49	3.00	0.00	876251.51	612.00	1.49	102.00	66969.03	1.00	422.00	
90	26.60	7853.98	4.00	0.00	876251.51	612.00	1.49	102.00	63042.04	1.00	433.40	

Table 2
Statistics of experimental data.

		f_c	A_D	n	$A_{tr,r}f_{y,r}$	$A_{tr}f_y$	$A_b(t_{sc}h_{sc})$	b/h_{sc}	h_{sc}	A_F	α	q_{exp}
Total data	No. of data	90	90	90	90	90	90	90	90	90	90	90
	Min	20.91	0.00	0.00	0.00	0.00	137.50	1.20	25.00	8831.77	0.00	13.14
	Max	52.60	9817.48	5.00	281486.70	876251.51	1950.00	3.60	150.00	112993.36	1.00	774.20
	μ	29.93	3812.31	2.27	30809.34	478005.92	1283.36	1.60	108.02	69782.55	0.88	399.38
	σ	8.09	3151.97	1.40	69124.83	342898.51	546.02	0.77	35.00	29475.67	0.33	174.26
	CV	0.27	0.83	0.62	2.24	0.72	0.43	0.48	0.32	0.42	0.38	0.44
Training data	No. of data	76	76	76	76	76	76	76	76	76	76	76
	Min	20.91	0.00	0.00	0.00	0.00	137.50	1.20	25.00	8831.77	0.00	13.14
	Max	51.90	9817.48	5.00	281486.70	876251.51	1950.00	3.60	150.00	112993.36	1.00	774.20
	μ	29.70	3700.83	2.21	30750.51	475217.38	1283.99	1.59	107.89	70424.49	0.88	396.96
	σ	7.74	3132.06	1.41	68251.42	341919.29	539.79	0.76	34.71	29599.29	0.33	173.33
	CV	0.26	0.85	0.64	2.22	0.72	0.42	0.48	0.32	0.42	0.37	0.44
Testing data	No. of data	14	14	14	14	14	14	14	14	14	14	14
	Min	20.91	0.00	0.00	0.00	0.00	137.50	1.20	25.00	9398.83	0.00	61.20
	Max	52.60	9503.32	4.00	281486.70	876251.51	1875.00	3.60	150.00	112993.36	1.00	692.20
	μ	31.16	4417.53	2.57	31128.70	493143.67	1279.93	1.64	108.71	66297.73	0.86	412.51
	σ	10.03	3309.67	1.40	76406.13	360833.07	600.06	0.84	37.87	29631.55	0.36	185.33
	CV	0.32	0.75	0.54	2.45	0.73	0.47	0.51	0.35	0.45	0.42	0.45

The regularisation method modifies the performance function, normally chosen to be the sum of squares of the network errors pertaining to the training set:

$$F = mse = \frac{1}{N}\sum_{i=1}^{N}(e_i)^2 = \frac{1}{N}\sum_{i=1}^{N}(t_i - \alpha_i)^2 \tag{9}$$

Generalisation is likely to be improved if the performance function is modified by adding a term including the mean of the sum of squares of weights and biases:

$$msereg = \gamma mse + (1-\gamma)msw \tag{10}$$

in which γ is the performance ratio, and $msw = \frac{1}{n}\sum_{j=1}^{n}\omega_j^2$. Using this performance function leads to smaller weights and biases and also causes the response to be less likely to overfit; however, determining the optimal regularisation parameter is a hard work. One approach to deal with the issue is the Bayesian framework of David MacKay [36], which has been implemented in the function "trainbr" of MATLAB software. Bayesian regularisation divides data set into two subsets: training and test cases. Therefore, Bayesian regularisation is known to provide superior generalisation performance than early stopping techniques, dividing the dataset into three subsets, when the data set is relatively small [35,37].

4. Dataset

Table 1 lists 90 records considered in this research. The data were taken from the tests conducted by Vianna et al. [3,38], Ahn et al. [17], Oguejiofor et al. [2,9], Cândido-Martins et al. [4], Kim and Choi [1], and Costa-Neves et al. [5]. The data were divided into two categories; the train and the test subsets including 76 and 14 data, respectively.

The "train" subset is used for computing the gradient and updating the network weights and biases. The error of test subset is not used in the training process; however, it is used to compare different models [35]. Table 2 stands for the statistical parameters regarding total, training, and test data.

5. Selection of input parameters

According to Lee and Lee [39], different inputs could be combined in different ways due to the fact that they could better reflect the physical mechanism than separated inputs. Experimental findings reveal that the shear strength of the PRSC is proportional to concrete dowels area ($A_D = n\pi\frac{D^2}{4}$), cross section of connector at the end-bearing zone ($A_b = h_{sc}t_{sc}$), tensile force in reinforcement bars ($A_{tr}f_y$), compressive strength of concrete (f_c), the thickness of concrete slab (b), and the friction between the concrete and the plate; this means the input ($A_{tr}f_y$), for instance, could better represent the physical mechanism of the shear

Table 3
ANNs architecture.

No.	Model	Input parameters	No. of inputs	No.	Model	Input parameters	No. of inputs
1	10BR1-1	f_c,A_D,n,A_{tr},$r f_y$,$A_{tr,wr} f_y$,	10	42	5BR1-1	f_c,A_D,n,$A_{tr} f_y$,$t_{sc} h_{sc}$	5
2	10BR2-1	$t_{sc} h_{sc}$,b/h_{sc},h_{sc},A_F,α	10	43	5BR2-1		5
3	10BR3-1		10	44	5BR3-1		5
4	10BR4-1		10	45	5BR4-1		5
5	10BR5-1		10	46	5BR5-1		5
6	10BR6-1		10	47	5BR6-1		5
7	9BR1-1	f_c,A_D,n,A_{tr},$r f_y$,$A_{tr,wr} f_y$,	9	48	5BR7-1		5
8	9BR2-1	$t_{sc} h_{sc}$,b/h_{sc},h_{sc},A_F	9	49	5BR8-1		5
9	9BR3-1		9	50	5BR9-1		5
10	9BR4-1		9	51	5BR1-2	f_c,A_D,$A_{tr} f_y$,$t_{sc} h_{sc}$,h_{sc}	5
11	9BR5-1		9	52	5BR2-2		5
12	9BR6-1		9	53	5BR3-2		5
13	8BR1-1	f_c,A_D,n,A_{tr},$r f_y$,$A_{tr,wr} f_y$,	8	54	5BR4-2		5
14	8BR2-1	$t_{sc} h_{sc}$,b/h_{sc},h_{sc}	8	55	5BR5-2		5
15	8BR3-1		8	56	5BR6-2		5
16	8BR4-1		8	57	5BR7-2		5
17	8BR5-1		8	58	5BR8-2		5
18	8BR6-1		8	59	5BR9-2		5
19	8BR7-1		8	60	4BR1-1	f_c,A_D,$A_{tr} f_y$,$t_{sc} h_{sc}$	4
20	8BR1-2	f_c,A_D,n,A_{tr},$r f_y$,$A_{tr,wr} f_y$,	8	61	4BR2-1		4
21	8BR2-2	$t_{sc} h_{sc}$,h_{sc},A_F	8	62	4BR3-1		4
22	8BR3-2		8	63	4BR4-1		4
23	8BR4-2		8	64	4BR5-1		4
24	8BR5-2		8	65	4BR6-1		4
25	8BR6-2		8	66	4BR7-1		4
26	8BR7-2		8	67	4BR8-1		4
27	7BR1-1	f_c,A_D,n,A_{tr},$r f_y$,$A_{tr,wr} f_y$,	7	68	4BR9-1		4
28	7BR2-1	$t_{sc} h_{sc}$,h_{sc}	7	69	4BR10-1		4
29	7BR3-1		7	70	4BR11-1		4
30	7BR4-1		7	71	3BR1-1	$\sqrt{f_c} A_D$,$A_{tr} f_y$,$t_{sc} h_{sc} f_c$	3
31	7BR5-1		7	72	3BR2-1		3
32	7BR6-1		7	73	3BR3-1		3
33	7BR7-1		7	74	3BR4-1		3
34	6BR1-1	f_c,A_D,n,$A_{tr} f_y$,$t_{sc} h_{sc}$,h_{sc}	6	75	3BR5-1		3
35	6BR2-1		6	76	3BR6-1		3
36	6BR3-1		6	77	3BR7-1		3
37	6BR4-1		6	78	3BR8-1		3
38	6BR5-1		6	79	3BR9-1		3
39	6BR6-1		6	80	3BR10-1		3
40	6BR7-1		6	81	3BR11-1		3
41	6BR8-1		6	82	3BR12-1		3
				83	3BR13-1		3

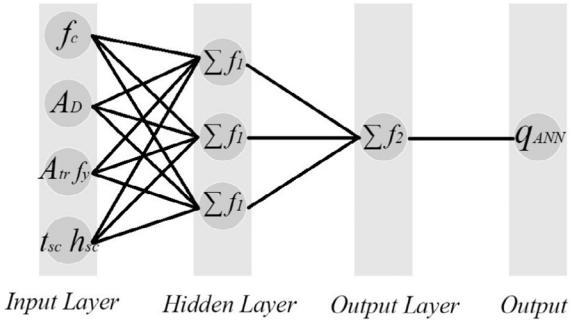

Fig. 3. The schematic architecture of 4BR3-1.

strength of PRSC than separate inputs A_{tr} and f_y. So different inputs and their combinations were selected according to equations mentioned in Section 2 and were considered to analyse their effectiveness in the shear strength of PRSC.

Therefore, this study considers 85 distinct architectures to detect the central terms. To model the elimination of end-bearing force, architectures with 10 inputs consider $\alpha = 0$ whereas architectures with fewer inputs consider $A_b = 0$. Table 3 shows the architectures and input parameters; all ANN architectures are labelled as n_1BRn_2-n_3 in which n_1, n_2, n_3 respectively denote the number of neurones, inputs, and series. Fig. 3 demonstrates the schematic architecture of 4BR3-1.

6. Modelling of the PRSC and training algorithm

The performance of ANNs significantly depends on the initial weights and biases. Therefore, 85 models (with different inputs and initial weights) based upon feed-forward backpropagation neural networks were constructed to attain the more accurate model taking account of the most effectual inputs. They were also trained by the function “trainbr”, comprehensively explained in Section 3.2. The “trainbr” uses Bayesian Regularisation Backpropagation (BRB) training algorithm, providing strong estimation for noisy and difficult inputs. BRB algorithm effectually eliminates network weights with small effects on the problem’s solution and shows superb performance by avoiding local minimums [40].

It is important to note that the training process was first initiated with 10 inputs, and each input was eliminated after training each architecture to analyse its effectiveness in the shear strength of PRSC; that is, the effectiveness of each parameter was considered in the inputs of the next architecture. In case a parameter was ineffective it was eliminated from inputs otherwise it was included in the inputs of the next architecture. Moreover, the higher threshold to the number of neurones was determined according to the condition in which the total number of weights and biases of the network was not greater than the

Table 4
Statistical parameters corresponding to different ANN architectures.

No.	Model	μ	σ	CV	No. of solution	No.	Model	μ	σ	CV	No. of solution
1	10BR1-1	0.0062	1.7E−06	2.8E−04	1	42	5BR1-1	0.0067	4.3E−06	6.5E-04	1
2	10BR2-1	0.0062	1.1E-04	1.8E-02	4	43	5BR2-1	0.0060	6.0E-04	1.0E−01	5
3	10BR3-1	0.0061	4.9E−04	8.0E−02	2	44	5BR3-1	0.0052	9.0E−08	1.7E−05	1
4	10BR4-1	0.0059	8.8E−04	1.5E−01	4	45	5BR4-1	0.0053	3.3E−04	6.2E−02	4
5	10BR5-1	0.0058	9.2E−04	1.6E−01	7	46	5BR5-1	0.0060	1.2E−03	2.1E−01	6
6	10BR6-1	0.0061	6.8E−04	1.1E−01	7	47	5BR6-1	0.0058	9.1E−04	1.6E−01	9
7	9BR1-1	0.0063	4.9E−06	7.8E−04	1	48	5BR7-1	0.0060	1.3E−03	2.1E−01	9
8	9BR2-1	0.0064	2.3E−04	3.6E−02	3	49	5BR8-1	0.0063	2.0E−03	3.2E−01	13
9	9BR3-1	0.0058	1.4E−04	2.4E−02	2	50	5BR9-1	0.0068	2.1E−03	3.1E−01	13
10	9BR4-1	0.0042	3.4E−04	8.1E−02	4	51	5BR1-2	0.0068	5.0E−06	7.3E−04	1
11	9BR5-1	0.0057	6.2E−04	1.1E−01	6	52	5BR2-2	0.0051	2.8E−04	5.6E−02	4
12	9BR6-1	0.0053	9.1E−04	1.7E−01	7	53	5BR3-2	0.0053	3.3E−04	6.2E−02	2
13	8BR1-1	0.0064	4.4E−06	6.8E−04	1	54	5BR4-2	0.0066	1.9E−04	2.8E−02	3
14	8BR2-1	0.0047	3.9E−05	8.3E−03	2	55	5BR5-2	0.0191	7.5E−03	3.9E−01	8
15	8BR3-1	0.0096	7.5E−06	7.8E−04	1	56	5BR6-2	0.0310	1.9E−02	6.1E−01	11
16	8BR4-1	0.0104	9.2E−04	8.8E−02	2	57	5BR7-2	0.0083	3.0E−03	3.6E−01	12
17	8BR5-1	0.0091	2.9E−03	3.2E−01	7	58	5BR8-2	0.0103	6.1E−03	5.9E−01	27
18	8BR6-1	0.0083	2.8E−03	3.4E−01	8	59	5BR9-2	0.0099	4.5E−03	4.5E−01	28
19	8BR7-1	0.0087	2.7E−03	3.0E−01	11	60	4BR1-1	0.0069	1.1E−05	1.6E−03	1
20	8BR1-2	0.0061	1.0E−05	1.7E−03	1	61	4BR2-1	0.0059	7.9E−04	1.3E−01	5
21	8BR2-2	0.0062	1.5E−04	2.5E−02	3	62	4BR3-1	0.0043	3.8E−11	8.9E−09	1
22	8BR3-2	0.0086	7.2E−04	8.4E−02	3	63	4BR4-1	0.0030	3.2E−07	1.1E−04	2
23	8BR4-2	0.0049	1.1E−03	2.3E−01	5	64	4BR5-1	0.0051	7.3E−04	1.4E−01	7
24	8BR5-2	0.0065	8.2E−04	1.3E−01	7	65	4BR6-1	0.0073	1.1E−03	1.5E−01	4
25	8BR6-2	0.0053	1.5E−04	2.8E−02	6	66	4BR7-1	0.0057	1.0E−03	1.8E−01	4
26	8BR7-2	0.0053	2.1E−04	4.0E−02	7	67	4BR8-1	0.0062	6.0E−04	9.7E−02	11
27	7BR1-1	0.0063	7.8E−06	1.2E−03	1	68	4BR9-1	0.0062	4.8E−04	7.7E−02	15
28	7BR2-1	0.0049	5.9E−06	1.2E−03	2	69	4BR10-1	0.0062	1.1E−05	1.8E−03	22
29	7BR3-1	0.0089	8.4E−04	9.5E−02	3	70	4BR11-1	0.0062	1.0E−03	1.7E−01	18
30	7BR4-1	0.0086	2.6E−03	3.0E−01	5	71	3BR1-1	0.0057	9.5E−06	1.7E−03	1
31	7BR5-1	0.0071	3.8E−03	5.4E−01	6	72	3BR2-1	0.0052	1.9E−06	3.6E−04	1
32	7BR6-1	0.0063	2.6E−03	4.1E−01	10	73	3BR3-1	0.0041	1.2E−04	2.8E−02	4
33	7BR7-1	0.0052	1.5E−03	2.9E−01	12	74	3BR4-1	0.0042	4.1E−04	9.8E−02	4
34	6BR1-1	0.0069	7.6E−06	1.1E−03	1	75	3BR5-1	0.0048	1.4E−03	2.8E−01	11
35	6BR2-1	0.0047	5.6E−07	1.2E−04	1	76	3BR6-1	0.0045	5.9E−04	1.3E−01	13
36	6BR3-1	0.0055	3.6E−04	6.6E−02	2	77	3BR7-1	0.0042	1.3E−03	3.2E−01	14
37	6BR4-1	0.0115	1.5E−03	1.3E−01	4	78	3BR8-1	0.0043	7.0E−04	1.6E−01	13
38	6BR5-1	0.0180	6.3E−03	3.5E−01	9	79	3BR9-1	0.0041	7.7E−04	1.9E−01	13
39	6BR6-1	0.0207	5.1E−03	2.4E−01	11	80	3BR10-1	0.0042	8.6E−04	2.0E−01	20
40	6BR7-1	0.0122	2.4E−03	2.0E−01	12	81	3BR11-1	0.004	6.2E−04	1.6E−01	17
41	6BR8-1	0.0129	3.4E−03	2.6E−01	18	82	3BR12-1	0.0042	7.5E−04	1.8E−01	19
						83	3BR13-1	0.0038	3.5E−04	9.3E−02	15

Note: $\mu = \frac{\sum_{i=1}^{n_s} NMSE_i}{n_s}$ where n_s is the number of specimens; $\sigma = \sqrt{(\sum_{i=1}^{n_s} NMSE_i - \mu)^2 / n_s}$; $CV = \frac{\sigma}{\mu}$.

Table 5
Summary of NMSE and R for the network with a unique solution.

Model	R			NMSE	
	All data	Training data	Testing data	Training data	Testing data
10BR1-1	0.9243	0.9204	0.9435	0.0078	0.0062
9BR1-1	0.9223	0.9183	0.9431	0.0081	0.0063
8BR1-1	0.9222	0.9182	0.9428	0.0081	0.0064
8BR3-1	0.9619	0.9720	0.9094	0.0028	0.0096
8BR1-2	0.9223	0.9178	0.9461	0.0081	0.0061
7BR1-1	0.9217	0.9175	0.9447	0.0081	0.0063
6BR1-1	0.9139	0.9092	0.9414	0.0089	0.0069
6BR2-1	0.9391	0.9354	0.9592	0.0064	0.0047
5BR1-1	0.9145	0.9096	0.9429	0.0088	0.0067
5BR3-1	0.9577	0.9588	0.9547	0.0041	0.0052
5BR1-2	0.9142	0.9095	0.9416	0.0089	0.0068
4BR1-1	0.9144	0.9098	0.9419	0.0088	0.0069
4BR3-1	0.9565	0.9557	0.9619	0.0044	0.0043
3BR1-1	0.9227	0.9175	0.9533	0.0081	0.0057
3BR2-1	0.9352	0.9316	0.9556	0.0068	0.0052

Note: NMSE = Normalize mean square error; R = Pearson correlation coefficient.

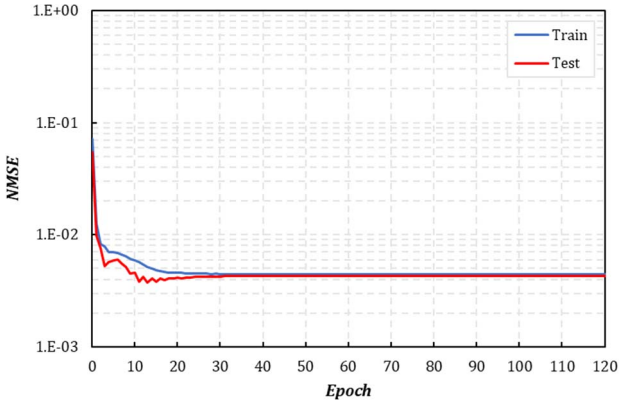

Fig. 4. Performance of 4BR3-1.

number of training examples [41,42]. Regarding the application of neural networks in engineering problems, a large number of presentations and publications suffer from a misconception [41]. Therefore, in this paper, determining the number of solutions pertaining to each architecture was considered to be an effectual remedy for the common mistake noted by Carpenter and Barthelemy [41], and each network was reinitialized with 100 different weights and biases to find the majority of solutions.

In short, parameters of the networks were as follows: number of neurones in the input and the hidden layers respectively ranged from 4

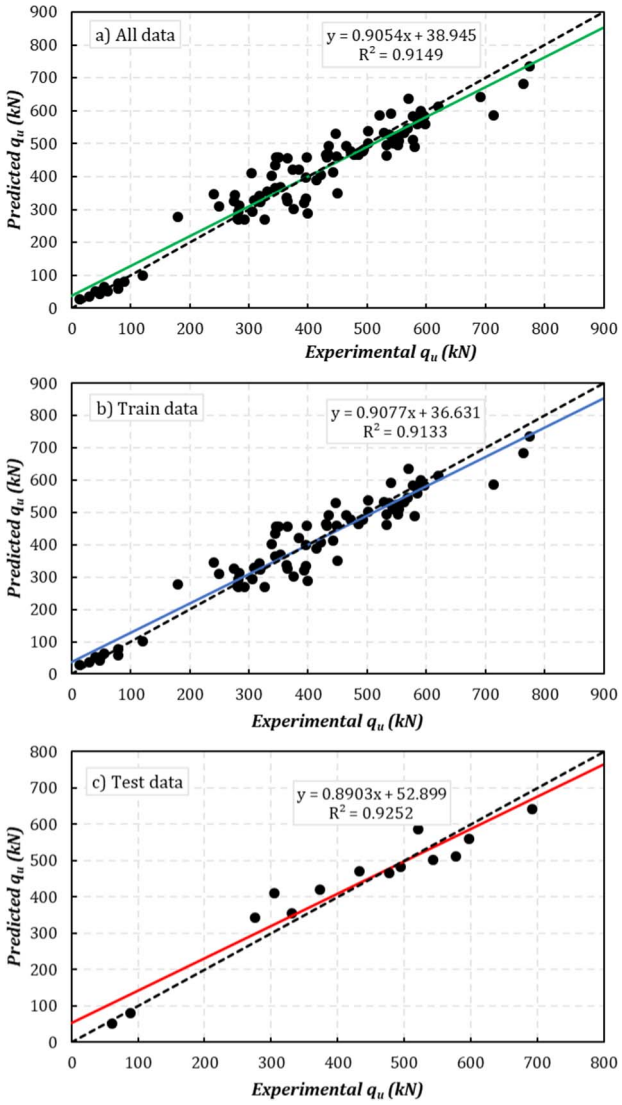

Fig. 5. Regressions of 4BR3-1 for (a) all data (b) train data (c) test data.

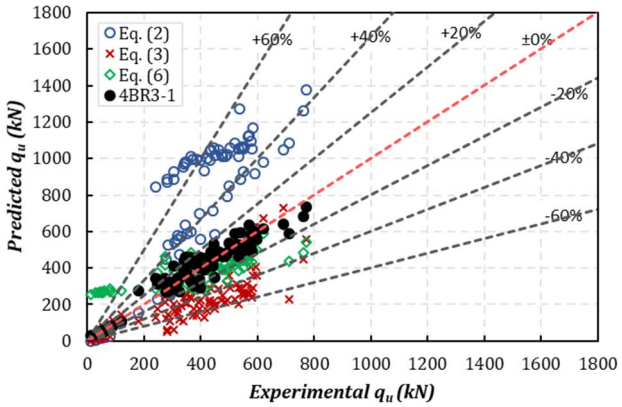

Fig. 6. Predicted and experimental shear strengths: a comparison between Eqs. (2), (3), (6) and 4BR3-1 model.

to 10 and 1 to 12, maximum epochs used for training process were 500, type of backpropagation was Bayesian regulation, initial adaptive value (mu) set to 1, mu increase and decrease factors respectively set to 1.5 and 0.8, the performance goal set to 0, the minimum performance gradient set to 10^{-7}, transfer functions in the hidden and output layers respectively set to $TANSIG(n) = \frac{2}{1+e^{-2n}} - 1$, generating values between

Table 6
Distribution of error percentages for different models.

Error (%)	Eq. (2)	Eq. (3)	Eq. (6)	4BR3-1
± 5	8 (9%)	1 (1%)	14 (16%)	27 (30%)
± 10	15 (17%)	5 (6%)	28 (31%)	51 (57%)
± 15	20 (22%)	8 (9%)	33 (37%)	62 (69%)
± 20	21 (23%)	9 (10%)	49 (54%)	75 (83%)
± 25	22 (24%)	15 (17%)	59 (66%)	80 (89%)
± 30	23 (26%)	22 (24%)	70 (78%)	84 (93%)
± 35	23 (26%)	28 (31%)	73 (81%)	87 (97%)
± 40	23 (26%)	34 (38%)	75 (83%)	87 (97%)
± 45	25 (28%)	44 (49%)	75 (83%)	88 (98%)
± 50	25 (28%)	52 (61%)	76 (84%)	88 (98%)
± 55	27 (30%)	64 (71%)	77 (86%)	89 (99%)
± 60	31 (34%)	72 (80%)	78 (87%)	89 (99%)
± 65	34 (38%)	79 (88%)	78 (87%)	89 (99%)
± 70	40 (44%)	82 (91%)	79 (88%)	89 (99%)
± 75	43 (48%)	84 (93%)	79 (88%)	89 (99%)
± 80	47 (52%)	87 (97%)	79 (88%)	89 (99%)
± 85	51 (57%)	89 (99%)	79 (88%)	89 (99%)
± 90	52 (58%)	89 (99%)	79 (88%)	89 (99%)
± 95	56 (62%)	89 (99%)	79 (88%)	89 (99%)
± 100	62 (69%)	90 (1 0 0)	79 (88%)	89 (99%)

Table 7
The effect of each variable on the shear strength of Perfobond connectors (typically 388.10 kN).

Input		Shear strength	
Name	Range	Range	Percent change
f_c	20.91 → 56.60	328.12 → 470.50	37%
A_D	0.00 → 9817.48	282.96 → 498.96	56%
$A_{tr} f_y$	0.00 → 1063961.67	363.60 → 507.53	41%
A_b	0.00 → 1950.00	270.03 → 414.11	37%

-1 and $+1$, and $PURELIN(n) = n$, generating outputs between $-\infty$ and $+\infty$, and the performance function set to MSEREG (Eq. (10)), which is an improved the sum of squares of the network errors and incorporates the mean of sum of squares of weights and biases.

Owning to the fact that the "trainbr" works best with scaled data, the network's inputs and targets were scaled so that they fall almost in the range of -1 to 1 [35]. Overall, the performance of the developed ANNs was evaluated in terms of three aspects: the value of the normalised mean square of errors (NMSE) for test subset, the correlation coefficient (R) for test subset, and the number of solutions.

The optimal number of neurones in the hidden layer is usually determined through trial and error. In this study, however, a systematic procedure was implemented to detect the optimum number of hidden neurones. First, the number of hidden neurones was varied from 1 to (No. of examples in the train subsets − 1)/(number of inputs + 2) with 100 different initial weights for each neurone. Second, the number of solutions respecting each neurone was determined; it is mathematically proved that the networks with a unique solution are those having the same median and mean values to do with the test subset. Eventually, taking NMSE and R into account, the optimal number of neurones was chosen. Such procedure is superior to a trial and error procedure in which merely a single error statistic is considered at the output layer.

7. Results and discussions

7.1. Selection of the best architecture

Table 4 reflects statistical parameters of the performance on the test subset with 100 different initial weights and also indicates the number of solutions associated with each model (architecture). According to Carpenter and Barthelemy [41], the number of solutions plays a crucial

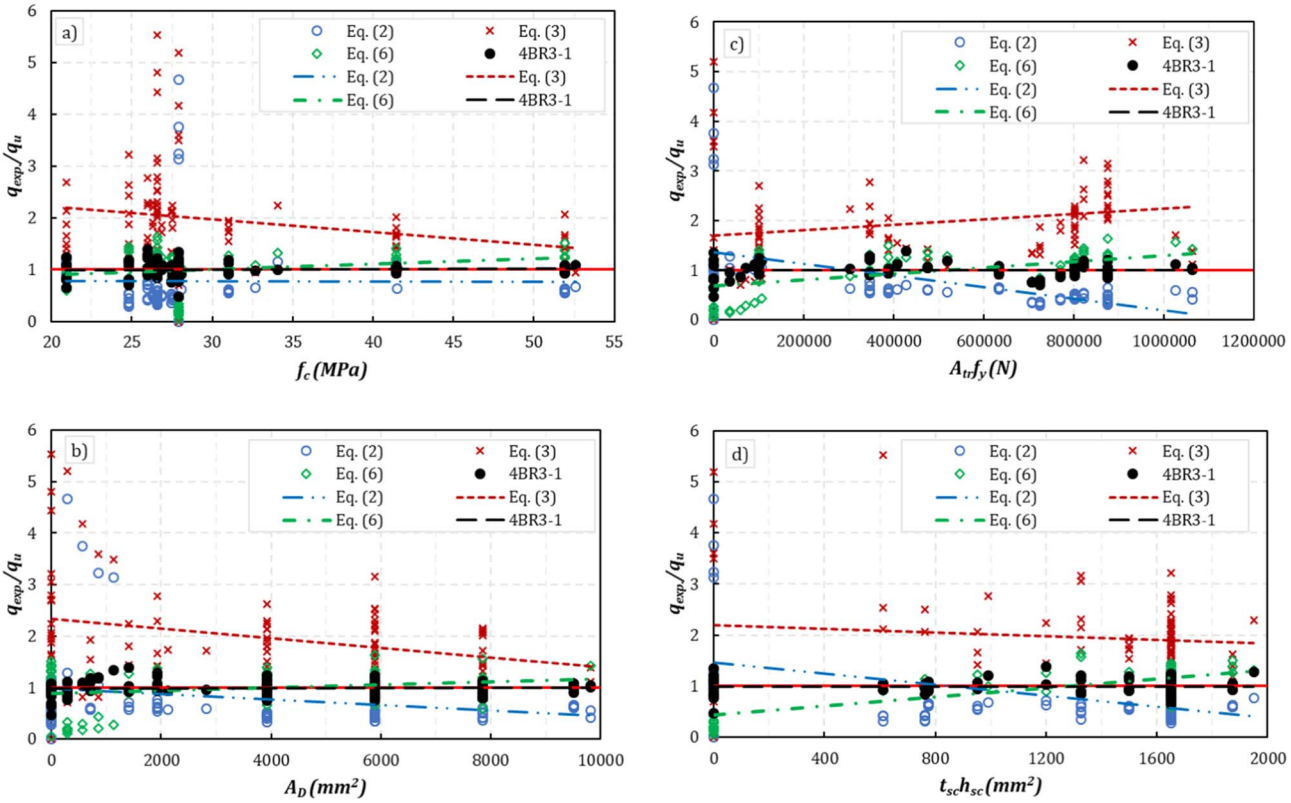

Fig. 7. Stability of different predictions for each parameter; (a) compressive strength (b) concrete dowels area (c) tensile force in transverse rebars (d) the cross-section of steel plate at the end-bearing zone.

role in opting for the best architecture.

From the statistical point of view, standard deviation (σ) and coefficient of variation $\left(CV = \frac{\sigma}{\mu}\right)$ are usually used to express the precision and repeatability of a test. A low value of σ implies that data points and the mean value (μ) of the set are very close to one another, whereas a high value of σ implies that data points are spread over a broader range of values. On the other hand, the coefficient of variation indicates the extent of variability of data points in terms of the mean value. Therefore, the smaller the standard deviation and coefficient of variation, the higher accuracy and the fewer the number of solutions.

According to Table 4, an increase in the number of neurones leads to a decrease in μ for different architectures. Nevertheless, smaller values of μ do not guarantee the better result. Therefore, standard deviation and coefficient of variation should be considered to ensure the unique solution. That is, the best architecture is the one with the smallest μ, σ, and CV. As shown in Table 4, the unique solutions could be found among the architectures with CV < 1.7E−03. From this table, it is anticipated that 4BR3-1 adequately fits the data with a unique solution (CV = 8.9E−09). Moreover, 4BR3-1 had a satisfactory mean value of the performance to do with the test subset (μ = 0.0043). Therefore, 4BR3-1 with merely four neurones in both input and hidden layers was considered to be the optimal model.

Moreover, after analysing the results listed in Table 4, it was concluded that it is not necessary to consider the bond effects incorporated in Eq. (4).

7.2. Neural network post-training analysis (regression)

Table 5 stands for R and NMSE values in terms of the architectures with a unique solution. Overall, network 4BR3-1 had the best R and NMSE to do with both the train and test subsets. Fig. 4 illustrates the variation of NMSE during the training process of 4BR3-1. In total, NMSE encountered a downward trend, indicating a satisfactory learning process. Fig. 5 indicates the graphical output provided by regression. In this figure, the dashed line demonstrates the perfect linear fit while the solid line illustrates the best linear fit. Fig. 5 represents a high R-Squared value (≈0.92) for all subsets, standing for an excellent correlation corresponding to 4BR3-1.

7.3. Validity of ANN model and empirical equations

The obtained results from ANN (4BR3-1) were compared with the aforementioned empirical equations to evaluate the capability of ANN in predicting the shear strength of PRSC; Fig. 6 and Table 6 reflect this comparison.

Fig. 6 illustrates experimental data against predicted data. The more deviation from the dashed line in red colour (0% error), the more inaccuracy. As shown in this figure, Eqs. (2) and (3) overestimates and underestimates the shear strength of Perfobond connectors, respectively. Eq. (6) has a higher accuracy in comparison with Eqs. (2) and (3); however, that is not as much accurate as 4BR3-1; it is plainly visible that the majority of predictions for 4BR3-1 lies in the range of −20 to +20 percent error, indicating a scientific precision for 4BR3-1.

Table 6 summarises the distribution of error percentages for different models. Regarding 4BR3-1, almost 90 percent of predicted results are within ± 25% of experimental results, while this figure is 24%, 17%, and 66% for Eqs. (2), (3), and (6), respectively. Moreover, 36% of the results derived by 4BR3-1 are within ± 5% of the experimental results whereas Eqs. (2), (3), and (6) reflect poor results in this range of error (± 5%). Although Eq. (6) represents satisfactory results in comparison to Eqs. (2) and (3), Table 6 indicates a sharp distinction between 4BR3-1 and Eq. (6). That is, the error percent of 98% of the results predicted by 4BR3-1 is less than 45% whereas 18% of the results derived by Eq. (6) have an error percent higher than 100%.

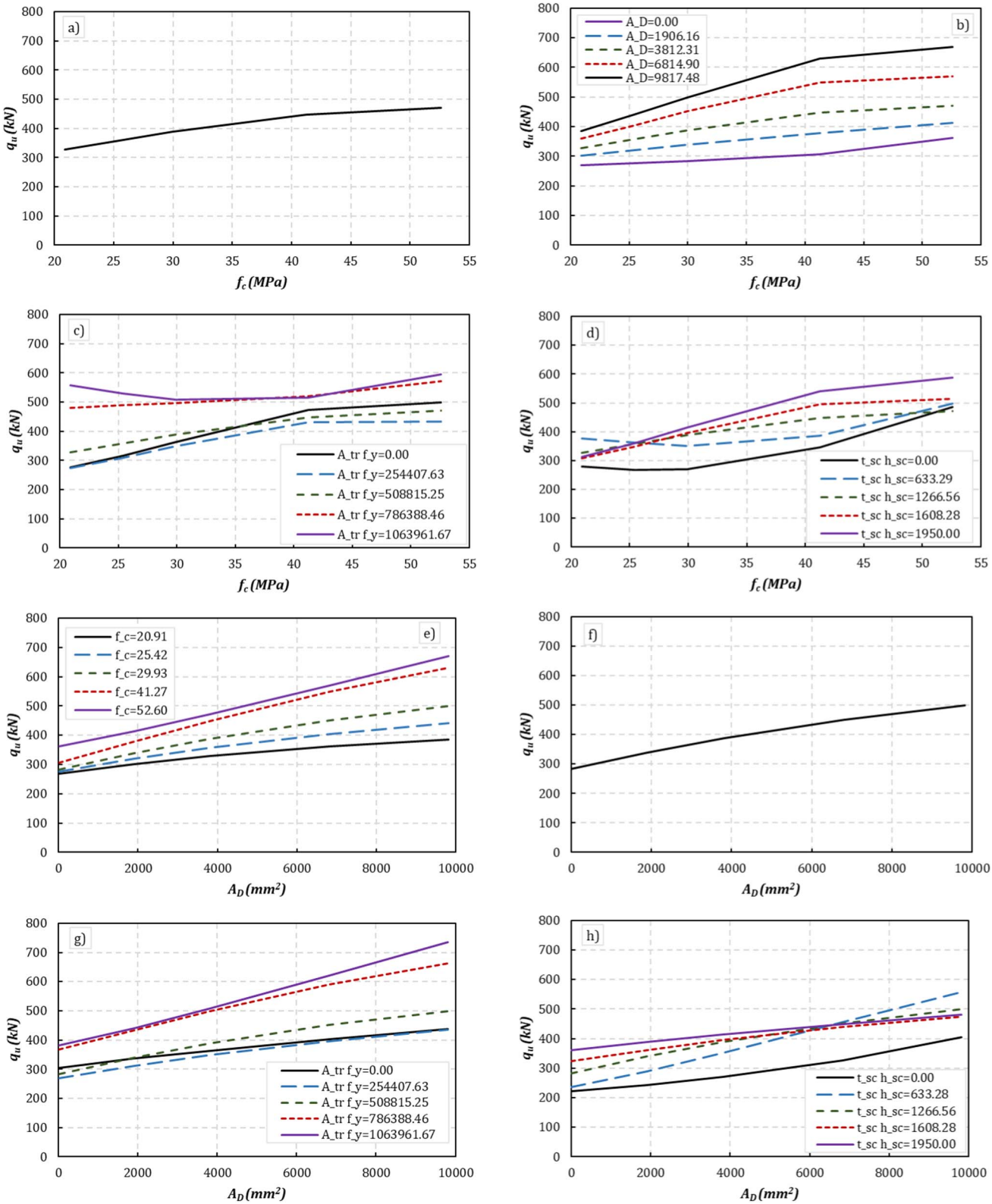

Fig. 8. Predicted shear strength versus different parameters: (a) variation of (f_c); (b) variations of (f_c) and (A_D); (c) variations of (f_c) and ($A_{tr}f_y$); (d) variations of (f_c) and ($t_{sc}h_{sc}$); (e) variations of (A_D) and (f_c); (f) variation of (A_D); (g) variations of (A_D) and ($A_{tr}f_y$); (h) variations of (A_D) and ($t_{sc}h_{sc}$); (i) variations of ($A_{tr}f_y$) and (f_c); (j) variations of ($A_{tr}f_y$) and (A_D); (k) variation of ($A_{tr}f_y$); (l) variations of ($A_{tr}f_y$) and ($t_{sc}h_{sc}$); (m) variations of ($t_{sc}h_{sc}$) and (f_c); (n) variations of ($t_{sc}h_{sc}$) and (A_D); (o) variations of ($t_{sc}h_{sc}$) and ($A_{tr}f_y$); (p) variation of ($t_{sc}h_{sc}$).

7.4. Sensitivity and stability analyses

The relative importance of each input variable can be assessed through the so-called sensitivity analysis. In this study, the sensitivity analysis of the inputs was conducted by monitoring the change in the shear strength of the PRSC, which was considered to be a percentage of the typical shear strength of the PRSC. The variable input ranged from the minimum value to the maximum value while others were constant

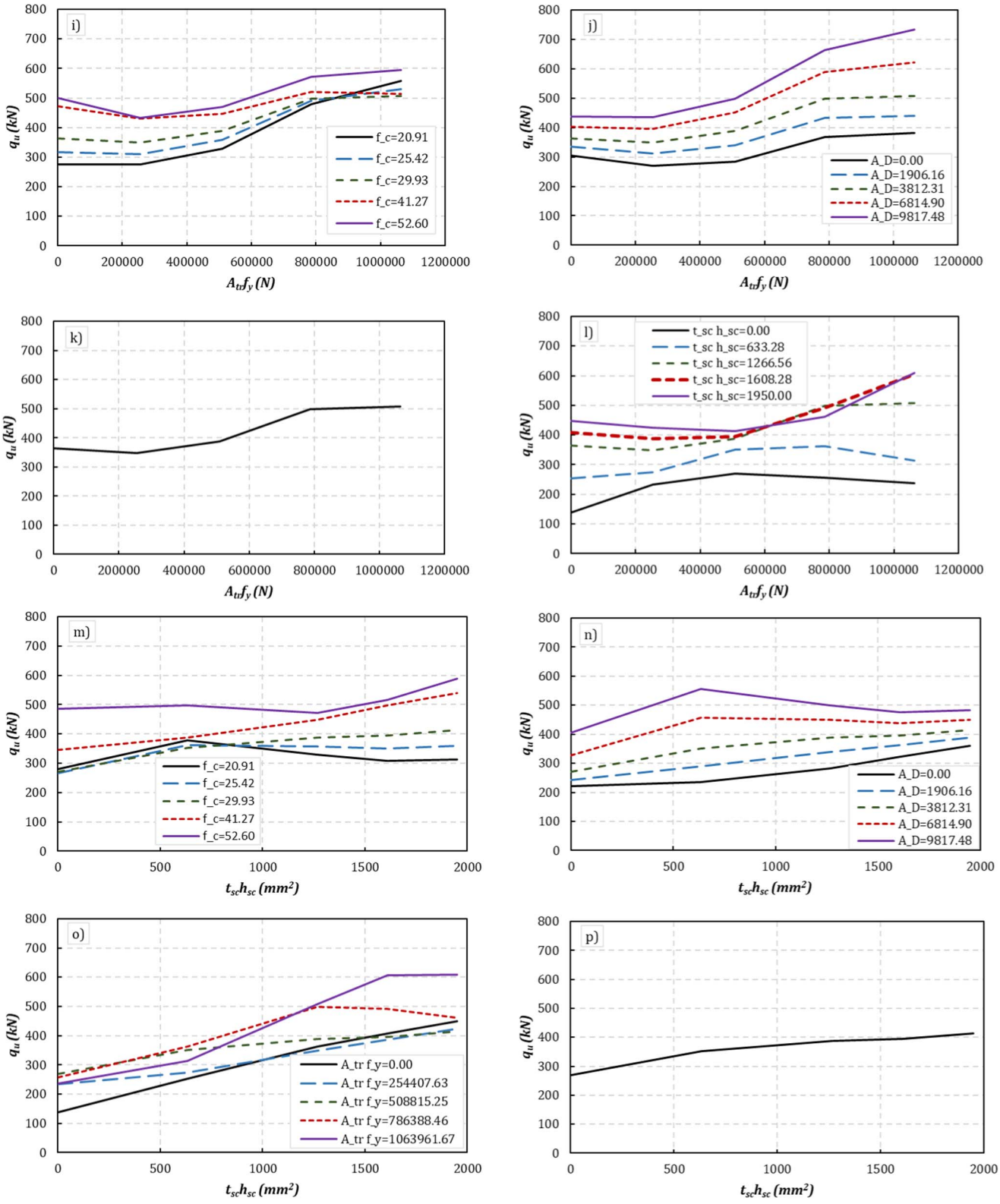

Fig. 8. (*continued*)

at their typical (median) values [43]. Table 7 summarises figures associated with the sensitivity analysis of input variables.

According to the results, the total area of the concrete dowels, with a 56% variation in q_u, plays a decisive role in the shear strength of PRSC. Moreover, a momentous change (41%) occurs in the shear strength with the variation in the total tensile force of reinforcement bars ($A_{tr}f_y$). Eventually, f_c and $A_b = t_{sc}h_{sc}$, with a 37% change in the shear strength of PRSC, take third place.

Fig. 7 indicates the stability of Eqs. (2), (3), and (6) as well as 4BR3-1 in terms of each input parameter. A stable prediction is considered to be related to the equation or model with the ratios of $q_{exp.}/q_u$ close to 1.0 (the solid line in red colour) for the entire range of each parameter's values. Fig. 7(a) indicates a stable trend of Eq. (2) for the change in f_c. Nonetheless, Eq. (2) overestimates the shear strength of PRSC in total.

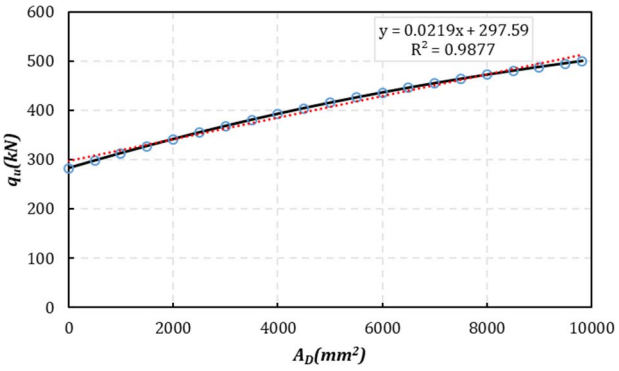

Fig. 9. The shear strength of Perfobond connector at reference parametric values.

Table 8
The reference values of parameters.

Parameter	Reference value
f_c	30
A_D	3800
$A_{tr}f_y$	508,800
A_b	1265

Fig. 7(b)–(d) stand for a downward trend of $q_{exp.}/q_u$ for Eq. (2) with regard to A_D, $A_{tr}f_y$, and $t_{sc}h_{sc}$, respectively. Moreover, Eq. (2) underestimates q_u for relatively lower values of $A_{tr}f_y$ or $t_{sc}h_{sc}$ whereas it overestimates q_u for relatively higher values of $A_{tr}f_y$ or $t_{sc}h_{sc}$. Eq. (3) reflects an unstable trend with respect to all parameters and, overall, underestimates the shear resistance of PRSC, as shown in Fig. 7. This figure also shows a satisfactory stability of Eq. (6) corresponding to f_c and A_D while representing instability of Eq. (6) regarding $A_{tr}f_y$ and $t_{sc}h_{sc}$. In Fig. 7(d), it is plainly visible that Eq. (6) overestimates the shear capacity of PRSC when the end-bearing force is eliminated from the end-bearing zone. Surprisingly, 4BR3-1 is so stable that the trend line lies on the red solid line, where experimental results and predicted results are relatively equal.

7.5. Parametric study of the shear strength of PRSC

Having a reliable neural network, one can conduct a parametric study to examine the effects of reinforcement bars, the compressive strength of the concrete, the cross-section of the steel plate at the end-bearing zone, and the area of concrete dowels on the shear strength of PRSC. In order to do the parametric study, a variable input varied from its minimum value to its maximum value while all other parameters were held constant at their typical values. 256 pushout specimens were simulated, as shown in Fig. 8. Fig. 8(a), (f), (k), and (p) reflect the shear strength of PRSC when f_c, A_D, $A_{tr}f_y$, and $t_{sc}h_{sc}$ range from their minimum value to their maximum value, respectively.

Overall, an increase in each parameter leads to a rise in the shear strength of PRSC. Fig. 8(b) represents a greater increment in the shear strength of PRSC when the compressive strength of concrete augments at higher values of A_D. Likewise, Fig. 8(e) illustrates a greater increase in the shear strength when the area of concrete dowels rises at a higher value of f_c. This fact indicates the importance of the combination of f_c and A_D, incorporated in empirical equations as the term $nD^2\sqrt{f'_c}$. As shown in Fig. 8(c), the variation of f_c encounters a similar trend; however, the trend is somewhat different for higher values of $A_{tr}f_y$, which is attributed to the lack of adequate data in the range of median to the maximum value of $A_{tr}f_y$. This similar trend places an emphasis that certain combinations of f_c and $A_{tr}f_y$ are not possible in estimating the shear strength of PRSC. Likewise, Fig. 8(g) shows that certain combinations of A_D and $A_{tr}f_y$ are not found. Fig. 8(d) and (m) indicate irregular trends for the variation of f_c at different values of $t_{sc}h_{sc}$, and vice versa, confirming the effect of the term $h_{sc}t_{sc}f_c$ used in empirical equations. Similarly, Fig. 8(h) and (l) suggest combinations of $t_{sc}h_{sc}$, A_D, and $A_{tr}f_y$, which have not been incorporated in the empirical equations.

8. A user-friendly equation to predict q_u

The derived results from ANN are in good agreement with the experimental data; nevertheless, employing the neural network in engineering design is not convenient on account of complex transfer functions. In order to address this problem, one practical approach is to substitute an empirical chart or equation generated by ANN for the equation directly derived from ANN. q_u is first plotted versus the parameter A_D out to a concern about the sensitivity of 4BR3-1 to A_D, as shown in Fig. 9. Meanwhile, other parameters remain constant at their reference values. Table 8 lists the reference value for each input parameter, chosen to be close to the median value. According to Leung et al. [44] and Naderpour et al. [45], to incorporate the effects of other parameters into the equation, a correction function (F) is derived as follows:

$$F(f_c, A_{tr}f_y, t_{sc}h_{sc}) = f_1(f_c).\, f_2(A_{tr}f_y).\, f_3(t_{sc}h_{sc}) = C_{f_c}.\, C_{A_{tr}f_y}.\, C_{t_{sc}h_{sc}} \tag{11}$$

Therefore, the variation of q_u with each parameter is supposed to be independent of other parameters. In order to derive the correction factors $(C_{f_c}.\, C_{A_{tr}f_y}.\, C_{t_{sc}h_{sc}})$, a group of curves, called Master Curves [44,45], are plotted using 4BR3-1 (Fig. 10). To attain an expression in terms of each correction factor, a particular correction factor is plotted against each parameter while all the other parameters remain constant at their reference values and, afterwards, a line fitting the curve with the minimum least square error is derived. Take, as an illustration, to derive C_{f_c}, a group of curves were plotted with a variation in $f_c/30$ (30 is the reference value of f_c indicated in Table 8) at different levels of $A_{tr}f_y$ and $t_{sc}h_{sc}$. Afterwards, these curves were divided by the value in which all parameters were fixed in their reference values (Fig. 10(a) and (b)). Eventually, a curve (Eq. (12)) that had the best fit to the Master Curves of Fig. 10(a) and (b) was constructed. Likewise, the following equations were attained:

$$C(f_c) = 1.0175\left(\frac{f_c}{30}\right)^{0.426} = 0.239 f_c^{0.426} \tag{12}$$

$$C(A_{tr}f_y) = 0.2132\left(\frac{A_{tr}f_y}{508800}\right) + 0.8201 = 4.19 \times 10^{-7} A_{tr}f_y + 0.8201 \tag{13}$$

$$C(t_{sc}h_{sc}) = 0.2882\left(\frac{t_{sc}h_{sc}}{1265}\right) + 0.7015 = 2.28 \times 10^{-4} t_{sc}h_{sc} + 0.7015 \tag{14}$$

The shear strength of PRSC (q_u) can then be derived from:

$$\begin{aligned} q_u &= (q_u)_{chart} C_{f_c} C_{A_{tr}f_y} C_{t_{sc}h_{sc}} = \left(0.0219\left(\frac{A_D}{3800}\right) + 297.59\right) C_{f_c} C_{A_{tr}f_y} C_{t_{sc}h_{sc}} \\ &= (1.44 \times 10^{-6} n\pi D^2 + 297.59)(0.239 f_c^{0.426})(4.19 \times 10^{-7} A_{tr}f_y \\ &\quad + 0.8201)(2.28 \times 10^{-4} t_{sc}h_{sc} + 0.7015) \end{aligned} \tag{15}$$

Fig. 11 compares the derived results from Eq. (15) and the experimental data associated with 90 data on the train and test subsets. From this figure, the shear strengths of PRSC computed by Eq. (15) are in reasonably good agreement with the experimental data. As shown in Fig. 11, Eq. (15) reflects a superb accuracy than Eq. (6), particularly, in terms of the specimens without end-bearing effect. The derivation of Eq. (15) is based upon a large number of data from the literature, and the equation is viable to the design of PRSC as long as the various parameters lie in the range of the data used for the neural network. Fig. 12 illustrates a comparison between Eqs. (2), (3), (6), (8), and 4BR3-1 model in the form of a histogram. Clearly, the 4BR3-1 model is the most accurate one, and its error ranges from −126 to 111 kN. Moreover, Eqs. (15) and (6) take second and third places, respectively.

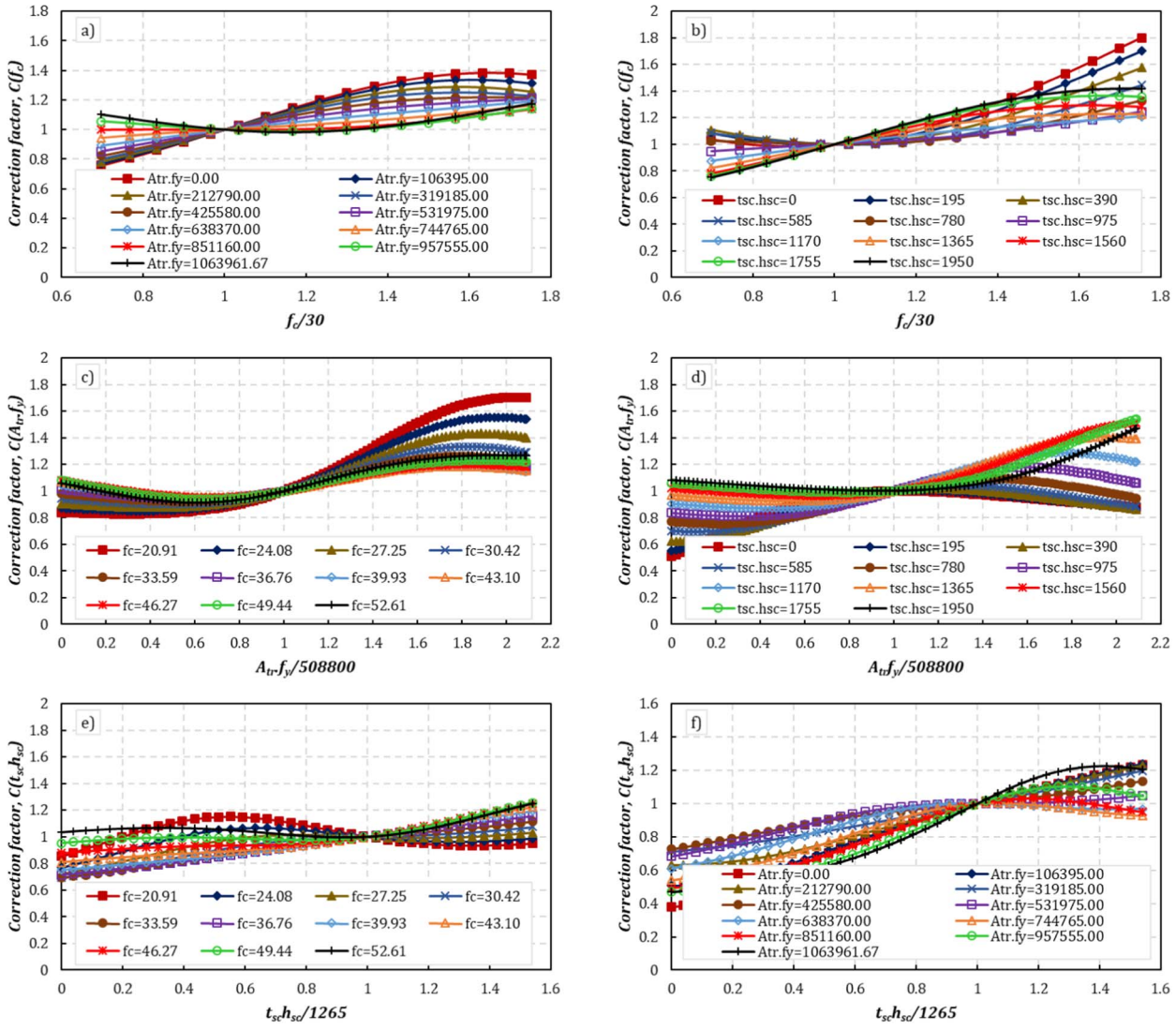

Fig. 10. Correction factors: (a) $C(f_c)$ with different $(A_{tr}f_y)$; (b) $C(f_c)$ with different $(t_{sc}h_{sc})$; (c) $C(A_{tr}f_y)$ with different (f_c); (d) $C(A_{tr}f_y)$ with different $(t_{sc}h_{sc})$; (e) $C(t_{sc}h_{sc})$ with different (f_c); (f) $C(t_{sc}h_{sc})$ with different $(A_{tr}f_y)$.

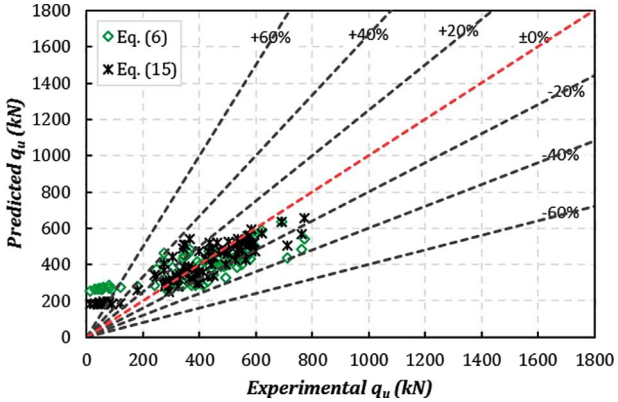

Fig. 11. Predicted and experimental shear strengths: a comparison between Eqs. (6) and (15).

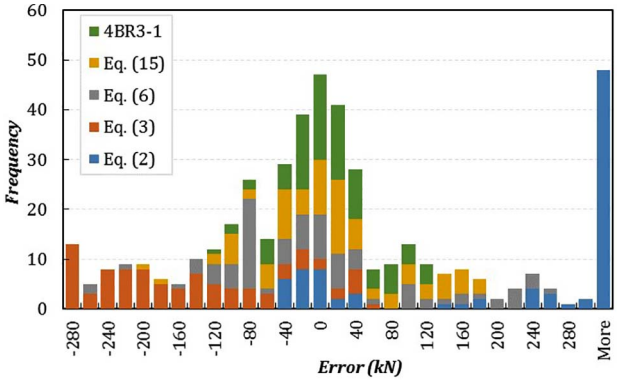

Fig. 12. The histogram of errors.

In other words, the error range of Eq. (15) is narrower than that of Eq. (6), indicating a higher accuracy and reliability for Eq. (15). It is plainly visible that Eq. (15) is simpler and more user-friendly than the AAN model and could be considered in practical designs. Nevertheless, the accuracy of the ANN model is much higher than Eq. (15) and, in spite of the complex structure of the ANN model, it could be employed for a more precise prediction of the shear strength of PRSC.

9. Summary and conclusions

In this study, 83 ANN-based models (each model was reinitialized 100 times) were presented. The number of inputs varied from 10 to 3

inputs. A parametric study and a sensitivity analysis were also conducted to investigate the impact of each input on the shear strength of PRSC. Having taken the analytical outcomes into account, the following conclusions can be drawn:

1. Developing neural networks revealed that the shear strength of PRSC is mainly related to four inputs encompassing the total area of concrete dowels (A_D), the concrete compressive strength (f_c), the total tensile force in transverse rebars ($A_{tr}f_y$), the cross-section of the steel plate ($t_{sc}h_{sc}$).
2. A large number of error statistics were used to detect the optimal number of hidden neurones; figures show the ANN model with three neurones in the hidden layer (4BR3-1) is capable of capturing the complex and nonlinear relationships in terms of the shear strength of PRSC.
3. A thorough investigation into the shear strength of PRSC was conducted in order to compare regression-based empirical equations with the ANN-based model. In comparison to the regression-based empirical equations, the ANN technique clearly excelled at predicting the shear resistant of PRSC. In other words, approximately 90% of the predicted results obtained from neural network were within ± 25% of the experimental results.

According to the sensitivity analysis, A_D, with a 56% variation in q_u, plays a decisive role in the shear strength of PRSC. Moreover, a momentous change (41%) occurs in the shear strength with the variation in $A_{tr}f_y$. In other words, A_D and $A_{tr}f_y$ take first and second place in the shear strength of PRSC whereas f_c and $t_{sc}h_{sc}$, with a 37% change in q_u, take third place.

Given the results of the parametric study, an increase in each input parameter led to an augmentation in the shear strength of PRSC. Overall, majority of assumptions incorporated in empirical equations were confirmed by the parametric study; however, ANN model did not conform to the empirical equations in all dimensions. This fact discloses that unknown relations could play a role beyond the shear strength of PRSC.

The 4BR3-1 model represented an excellent stability by retaining the mean value of $\frac{q_{exp}}{q_u}$ close to 1 on the whole range of four input parameters, while empirical equations reflected worse stability by deviating from 1.

Using a reliable ANN (4BR3-1), a user-friendly equation was derived in order to compute the shear strength of PRSC. Regarding 90 specimens, the user-friendly equation showed superior accuracy to existing empirical equations. Thus, a simple empirical equation, with higher accuracy, was introduced for the practical design of PRSC. However, the equation can be further improved by more experimental data in the future.

Eq. (15) provides a simple and user-friendly equation with a reasonable accuracy for practical design of PRSC; however, the ANN model has much higher accuracy than Eq. (15) and is useful for the cases in which higher precision is needed. Moreover, the higher accuracy of ANN with regard to the specimens with end-bearing effect is more outstanding than Eq. (15) and, in turn, ANN model could be more effectual in this case.

In conclusion, this study not only indicates the superiority of ANN in comparison to the conventional regression analysis but also introduce a user-friendly ANN-based equation to predict the shear resistance of PRSC.

References

[1] Kim S-H, Choi J-H. Experimental study on shear connection in unfilled composite steel grid bridge deck. J Constr Steel Res 2010;66:1339–44. http://dx.doi.org/10.1016/j.jcsr.2010.05.008.

[2] Oguejiofort EC, Hosaint MU. Numerical analysis of push-out specimens perfobond rib connectors. Comput Struct 1997;62.

[3] Vianna J da C, Costa-Neves LF, Vellasco PCG da S, de Andrade SAL. Experimental assessment of Perfobond and T-Perfobond shear connectors' structural response. J Constr Steel Res 2009;65:408–21.

[4] Cândido-Martins JPS, Costa-Neves LF, Vellasco PCG da S. Experimental evaluation of the structural response of Perfobond shear connectors. Eng Struct 2010;32:1976–85.

[5] Costa-Neves LF, Figueiredo JP, Vellasco PCG da S, da Cruz Vianna J. Perforated shear connectors on composite girders under monotonic loading: an experimental approach. Eng Struct 2013;56:721–37.

[6] Rodrigues JPC, Laím L. Behaviour of Perfobond shear connectors at high temperatures. Eng Struct 2011;33:2744–53.

[7] Zellner W. Recent designs of composite bridges and a new type of shear connectors. Compos. Constr. 1987:240–52.

[8] Vianna JC, Costa Neves LF, Vellasco P, Andrade SAL. Estudo Comparativo de Conectores de Corte para Estruturas Mistas de Aço e Betão. Construção Mag 2008;23:23–30.

[9] Oguejiofor EC, Hosain MU. A parametric study of perfobond rib shear connectors. Can J Civ Eng 1994;21:614–25. http://dx.doi.org/10.1139/l94-063.

[10] Al-Darzi SYK, Chen AR, Liu YQ. Finite element simulation and parametric studies of perfobond rib connector. Am J Appl Sci 2007;4:122–7.

[11] Ahn J, Kim S, Jeong Y. Shear behaviour of perfobond rib shear connector under static and cyclic loadings. Mag Concr Res 2008;60:347–57. http://dx.doi.org/10.1680/macr.2007.00046.

[12] Zheng S, Liu Y, Yoda T, Lin W. Parametric study on shear capacity of circular-hole and long-hole perfobond shear connector. J Constr Steel Res 2016;117:64–80.

[13] Allahyari H, Nikbin IM, Rahimi S, Allahyari A. Experimental measurement of dynamic properties of composite slabs from frequency response. Measurement 2018;114:150–61.

[14] Tang C-W. Radial basis function neural network models for peak stress and strain in plain concrete under triaxial stress. J Mater Civ Eng 2009;22:923–34.

[15] Jain A, Jha SK, Misra S. Modeling and analysis of concrete slump using artificial neural networks. J Mater Civ Eng 2008;20:628–33.

[16] Zhao Z, Ren L. Failure criterion of concrete under triaxial stresses using neural networks. Comput Civ Infrastruct Eng 2002;17:68–73.

[17] Ahn J-H, Lee C-G, Won J-H, Kim S-H. Shear resistance of the perfobond-rib shear connector depending on concrete strength and rib arrangement. J Constr Steel Res 2010;66:1295–307.

[18] Medberry SB, Shahrooz BM. Perfobond shear connector for composite construction. Eng J 2002;39:2–12.

[19] Veríssimo GS, Paes JLR, Valente I, Cruz PJS, Fakury RH. Design and experimental analysis of a new shear connector for steel and concrete composite structures; 2006.

[20] Al-Darzi S, Chen A, Liu Y. Development of new hole shape of perfobond shear connectors, parametric study. 2nd Int. Symp. Connect. between steel Concr; 2007. p. 1349–58.

[21] Hosaka T, Mitsuki K, Hiragi H, Ushijima Y, Tachibana Y, Watanabe H. An experimental study on shear characteristics of perfobond strip and it's rational strength equations. J Struct Eng 2000;46:1593–604.

[22] Company TDSB. The D. S. Brown Company An Introduction to : Exodermic™ Bridge Decks 2007:8 < http://www.exodermic.com/docs/pdf/brochure/ExoRev.pdf > .

[23] Karan FSN, Chakraborty S. Dynamics of a repulsive voter model. IEEE Trans Comput Soc Syst 2016;3:13–22.

[24] Karan FSN, Chakraborty S. Detecting behavioral anomaly in social networks using symbolic dynamic filtering. ASME 2015 Dyn. Syst. Control Conf., American Society of Mechanical Engineers; 2015, p. V003T37A001-V003T37A001.

[25] De Fenza A, Sorrentino A, Vitiello P. Application of Artificial Neural Networks and Probability Ellipse methods for damage detection using Lamb waves. Compos Struct 2015;133:390–403.

[26] Cascardi A, Micelli F, Aiello MA. An Artificial Neural Networks model for the prediction of the compressive strength of FRP-confined concrete circular columns. Eng Struct 2017;140:199–208.

[27] Rebouh R, Boukhatem B, Ghrici M, Tagnit-Hamou A. A practical hybrid NNGA system for predicting the compressive strength of concrete containing natural pozzolan using an evolutionary structure. Constr Build Mater 2017;149:778–89.

[28] Haykin S. Neural network: a comprehensive foundation. New York: Macmillan; 1994.

[29] Warnes MR, Glassey J, Montague GA, Kara B. Comparing different modeling techniques for the *Escherichia coli* fermentation process. In: Munack A, Schönert K, editors. Comput Appl Biotechnol. Garmisch-Partenkirchen, Germany: PERGAMON; 1995. p. 142–7.

[30] Hegazy T, Tully S, Marzouk H. A neural network approach for predicting the structural behavior of concrete slabs. Can J Civ Eng 1998;25:668–77.

[31] Elshafey AA, Haddara MR, Marzouk H. Damage detection in offshore structures using neural networks. Mar struct 2010;23:131–45.

[32] Elshafey AA, Rizk E, Marzouk H, Haddara MR. Prediction of punching shear strength of two-way slabs. Eng Struct 2011;33:1742–53.

[33] Elshafey AA, Dawood N, Marzouk H, Haddara M. Crack width in concrete using artificial neural networks. Eng Struct 2013;52:676–86.

[34] Fahmy AS, El-Madawy ME-T, Gobran YA. Using artificial neural networks in the design of orthotropic bridge decks. Alexandria Eng J 2016;55:3195–203.

[35] Beale M, Hagan M, Demuth H. Neural Network Toolbox-User's Guide (Vol. R2014a); 2014.

[36] MacKay DJC. Bayesian interpolation. Neural Comput 1992;4:415–47.

[37] Bashir R, Ashour A. Neural network modelling for shear strength of concrete members reinforced with FRP bars. Compos Part B Eng 2012;43:3198–207.

[38] Vianna J da C, de Andrade SAL, Vellasco PCG da S, Costa-Neves LF. Experimental study of Perfobond shear connectors in composite construction. J Constr Steel Res 2013;81:62–75.

[39] Lee S, Lee C. Prediction of shear strength of FRP-reinforced concrete flexural members without stirrups using artificial neural networks. Eng Struct 2014;61:99–112.
[40] Jazayeri K, Jazayeri M, Uysal S. Comparative analysis of Levenberg-Marquardt and Bayesian regularization Backpropagation algorithms in photovoltaic power estimation using artificial neural network. Ind Conf Data Min. Springer; 2016. p. 80–95.
[41] Carpenter WC, Barthelemy J-F. Common misconceptions about neural networks as approximators. J Comput Civ Eng 1994;8:345–58.
[42] Carpenter WC. Effect of design selection on response surface performance; 1993.
[43] Dias WPS, Pooliyadda SP. Neural networks for predicting properties of concretes with admixtures. Constr Build Mater 2001;15:371–9.
[44] Leung CK, Ng MY, Luk HC. Empirical approach for determining ultimate FRP strain in FRP-strengthened concrete beams. J Compos Constr 2006;10:125–38.
[45] Naderpour H, Kheyroddin A, Amiri GG. Prediction of FRP-confined compressive strength of concrete using artificial neural networks. Compos Struct 2010;92:2817–29.